

Article

Aloe Vera Functionalized Magnetic Nanoparticles Entrapped Ca Alginate Beads as Novel Adsorbents for Cu(II) Removal from Aqueous Solutions

Surbhi Lilhare ¹, Sunitha B. Mathew ^{1,*} , Ajaya Kumar Singh ^{1,2,*} and Sónia A. C. Carabineiro ³ ¹ Department of Chemistry, Govt. V. Y. T. PG Autonomous College, Durg, Chhattishgarh 491001, India² School of Chemistry & Physics, Westville Campus, University of KwaZulu-Natal, Durban 4000, South Africa³ LAQV-REQUIMTE, Department of Chemistry, NOVA School of Science and Technology, Universidade NOVA de Lisboa, 2829-516 Caparica, Portugal

* Correspondence: smathew@govtsciencecollegedurg.ac.in or sunithabmathew@gmail.com (S.B.M.);

ajayaksingh@govtsciencecollegedurg.ac.in or ajayaksingh_au@yahoo.co.in (A.K.S.);

Tel.: +91-94-2410-8409 (S.B.M.)

Abstract: CABs (Ca alginate beads), AVCABs (Aloe vera Ca alginate beads), and AVMNCABs (Aloe-vera functionalized magnetic nanoparticles entrapped Ca alginate beads) were developed as adsorbents for the removal of Cu(II) from aqueous solutions. The materials were characterized using Fourier-transform infrared (FTIR) spectroscopy, high-resolution scanning electron microscopic (HR-SEM) analysis, X-ray diffraction (XRD), energy-dispersive X-ray (EDX) spectroscopy, and a vibrating-sample magnetometer (VSM). The effect of several parameters, such as pH, time, temperature, adsorbent dose, etc., were investigated. The adsorption isotherm of Cu(II) was adjusted best to the Langmuir model. The maximum adsorption capacities were 111.11 mg/g, 41.66 mg/g, and 15.38 mg/g for AVMNCABs, AVCABs, and CABs, respectively. The study of the adsorption kinetics for Cu(II) ions on beads followed a pseudo-second-order kinetic model, with a very good correlation in all cases. The adsorption studies used a spectrophotometric method, dealing with the reaction of Cu(II) with KSCN and variamine blue.

Keywords: copper ion adsorption; magnetic nanoparticles; aloe-vera functionalized alginate beads; adsorption isotherm; spectrophotometric method



Citation: Lilhare, S.; Mathew, S.B.; Singh, A.K.; Carabineiro, S.A.C. Aloe Vera Functionalized Magnetic Nanoparticles Entrapped Ca Alginate Beads as Novel Adsorbents for Cu(II) Removal from Aqueous Solutions. *Nanomaterials* **2022**, *12*, 2947. <https://doi.org/10.3390/nano12172947>

Academic Editor: George Z. Kyzas

Received: 12 July 2022

Accepted: 15 August 2022

Published: 26 August 2022

Publisher's Note: MDPI stays neutral with regard to jurisdictional claims in published maps and institutional affiliations.



Copyright: © 2022 by the authors. Licensee MDPI, Basel, Switzerland. This article is an open access article distributed under the terms and conditions of the Creative Commons Attribution (CC BY) license (<https://creativecommons.org/licenses/by/4.0/>).

1. Introduction

Cu(II) is essential for the human body, but excessive intake can damage organs and, in extreme cases, lead to death. Copper is commonly used in roofing, plumbing, electroplating, utensils, pesticides, fertilizers, and medicines. It may also result from mining and industrial wastes. Exposure to high levels of copper or its intake through contaminated food, air, and water is dangerous [1,2]. The ingestion of high doses of copper can cause severe mucosal corrosion and irritation, central nervous system damage, followed by depression and intense capillary damage. It can also cause gastrointestinal irritation and the necrosis of liver and kidney tissues, leading to hepatic and renal damage due to chronic poisoning. The most serious situations are diseases such as leukemia, hepatitis, and Wilson's disease, among others. The World Health Organization recommends 1 mg L⁻¹ as the maximum acceptable limit of Cu(II) in drinking water [3].

Several methods, such as adsorption, reverse osmosis, chemical precipitation, ion exchange, membrane filtration, evaporation, and electrochemical procedures [4–7], have been reported for the treatment of wastewater. Among those, adsorption is promising for removing Cu(II) ions, given its operational ease, high efficiency, low cost, and good recyclability. Several types of adsorbents, such as zeolites [8], biomasses [9–15], fly ash [16], activated carbon [17–19], chitosan [20], polymeric hybrid sorbents [21–26], and agriculture

wastes [27] have been reported. A large number of the latter, namely orange peels [28], palm shells [29], sawdust [30], hazelnut shells [31], rice husk [32], walnut shells [33], etc., have been used as cheap adsorbents for removing Cu(II) from aqueous solutions.

Magnetic nanoparticles can be entrapped inside various organic and inorganic stabilizers, such as activated carbon [17–19], chitosan [34–37], alginate biopolymer [38,39], and β -cyclodextrin [40,41] to minimize their aggregation, enhance their adsorption efficiency, and enable the easy separation from the matrix. Sodium alginate is a water-soluble and commonly used natural polysaccharide with wide uses due to its non-toxic, inexpensive, biocompatible, biodegradable, emulsion stabilizing, and bioadhesive nature [42,43]. The alginates have the ability to form gels in the presence of calcium ions (Ca^{2+}), which occurs through the interaction and cross-linking between the L-guluronic acid (G) of alginate and the calcium ion (Ca^{2+}) in solution.

Aloe vera is a tropical, medicinal plant with a polysaccharide-rich matrix. It contains amino acids, lignin, salicylic acid, enzymes, vitamins, minerals, several carbohydrates, etc. Such molecules have functional groups that are able to bind with metals [44,45].

In this study, bio-sorbent AVMNCABs (Aloe-vera functionalized magnetic nanoparticles on Ca alginate beads) were prepared by mixing the pulp of Aloe vera leaves, a natural ingredient, with alginate and magnetic nanoparticles. Its efficiency for Cu(II) removal from aqueous solutions was compared with CABs (calcium alginate beads) and AVCABs (Aloe vera calcium alginate beads) using a simple spectrophotometric method. The performance and reusability of the adsorbents were investigated, and the influence of the temperature, time, and pH was studied in batch conditions. The thermodynamic and kinetic results revealed that the materials had advantages, such as a high adsorption capacity, simplicity, inexpensiveness, and good reproducibility. Adsorption isotherm models were used to explore the possibility of applying the synthesized adsorbents to the removal of Cu(II) ions from aqueous solutions. The study was carried out by a simple spectrophotometric procedure established in our laboratory and using potassium thiocyanate and variamine blue [46].

2. Materials and Methods

2.1. Reagents

The reagents used were of analytical grade. Double distilled water was used in all of the experiments. Copper sulfate (CuSO_4), ferrous chloride dihydrate ($\text{FeCl}_2 \cdot 2\text{H}_2\text{O}$), ferric chloride hexahydrate ($\text{FeCl}_3 \cdot 6\text{H}_2\text{O}$), and potassium thiocyanate (KSCN) were obtained from Merck (Mumbai, India). Variamine blue (VB) [0.05%], sodium alginate ($\text{C}_6\text{H}_9\text{NaO}_7$)—used for obtaining the alginate beads, and calcium chloride (CaCl_2), which was used for cross-linking the alginate beads—were obtained from Sigma-Aldrich (Mumbai, India). Moreover, 0.1 M sodium hydroxide (NaOH) and 0.1 M hydrochloric acid (HCl) were also prepared.

The Aloe vera leaves were collected from a nearby area, washed several times with double distilled water to remove dust and other impurities, and then cut into small pieces, followed by extraction of the gel.

2.2. Equipment

X-ray diffraction (XRD) analysis was carried out in an Expert-Pro PW3064/60 apparatus from 5° to 80° (Almelo, Netherlands). A Thermo Nicolet Avtar 370 Fourier-transform infrared (FT-IR) spectrometer (Tokyo, Japan) was used to record the infrared spectra in the $500\text{--}4000\text{ cm}^{-1}$ range with the help of KBr pellets. Scanning Electron Microscopic (SEM) images were obtained in a Jeol 6390LA/OXFORD XMX N (Tokyo, Japan) to analyze the surface morphology of the adsorbents. Energy-Dispersive X-ray (EDS/EDX) spectroscopy analysis (Oxford instruments, Abingdon, UK) was utilized to obtain the elemental composition. A vibrating-sample magnetometer (VSM) (Lake Shore 7410 model Westerville, OH, USA) was used to obtain the magnetization curve of the adsorbents. A Systronics ultraviolet-visible (UV-Vis) spectrophotometer-117 (Carry 50 scan, Varian, East Lyme, CT, USA) was used to measure the absorbance. The pH measurements were carried out on a

digital Systronics pH meter (112 model, Ahmedabad, India). The temperature was kept constant using a thermostatic water bath.

2.3. Preparation of Beads

2.3.1. Synthesis of Ca Alginate Beads (CABs)

Sodium alginate (SA) (1.5 g powder) was added to 50 mL of double distilled water. A viscous solution was obtained, which was added dropwise into a CaCl_2 (2%, *w/v*) solution with gentle stirring, resulting in the formation of the spherical bio-sorbent. The beads were then left for 24 h in the CaCl_2 solution to become stable and rinsed three times with distilled water to eliminate excess Ca(II) and stored in distilled water for subsequent use.

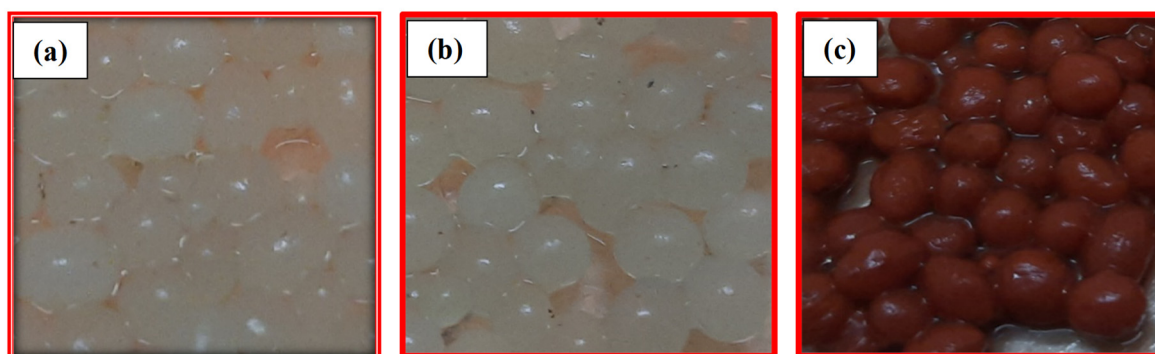
2.3.2. Synthesis of Aloe-Vera Calcium Alginate Beads (AVCABs)

The Aloe vera (AV) gel (0.25 g) was added to the viscous solution containing sodium alginate (1.5 g in 50 mL of distilled water). The solution thus obtained was added dropwise into CaCl_2 (2%, *w/v*) aqueous solution with stirring. The beads were then left for 24 h in the CaCl_2 solution to become stable. The gel beads were then washed three times with distilled water and stored in clean distilled water for further use.

2.3.3. Synthesis of Aloe-Vera Functionalized Magnetic Nanoparticles on Ca Alginate Beads (AVMNCABs)

The Fe_3O_4 nanoparticles (IN) were obtained by co-precipitation, mixing ferric chloride (Fe^{2+}) and ferrous chloride (Fe^{3+}) in a molar ratio of 2:1, followed by the addition of 1.5 M NH_4OH solution at room temperature ($\sim 30^\circ\text{C}$) under vigorous stirring. The nanoparticles were obtained as a black precipitate that was magnetically separated and then washed three times with double distilled water and dried at 200°C for 2 h.

The Fe_3O_4 nanoparticles (0.05 g) were added to the viscous solution containing 0.25 g of Aloe vera gel in a 3% aqueous sodium alginate solution. Later, the above mixture was added dropwise to the CaCl_2 solution, leading to the formation of AVMNCABs. The beads were then left for 24 h in the CaCl_2 solution to become stable. Then, they were washed three times with double distilled water and stored for later use in distilled water. The beads became red-brown due to the modified magnetic nanoparticles. The representative images of the gel beads (CABs, AVCABs, and AVMNCABs) are displayed in Figure 1A (their approximate size was 2–3 mm). The synthesis of the gel beads is represented in Figure 1B.



(A)

Figure 1. Cont.

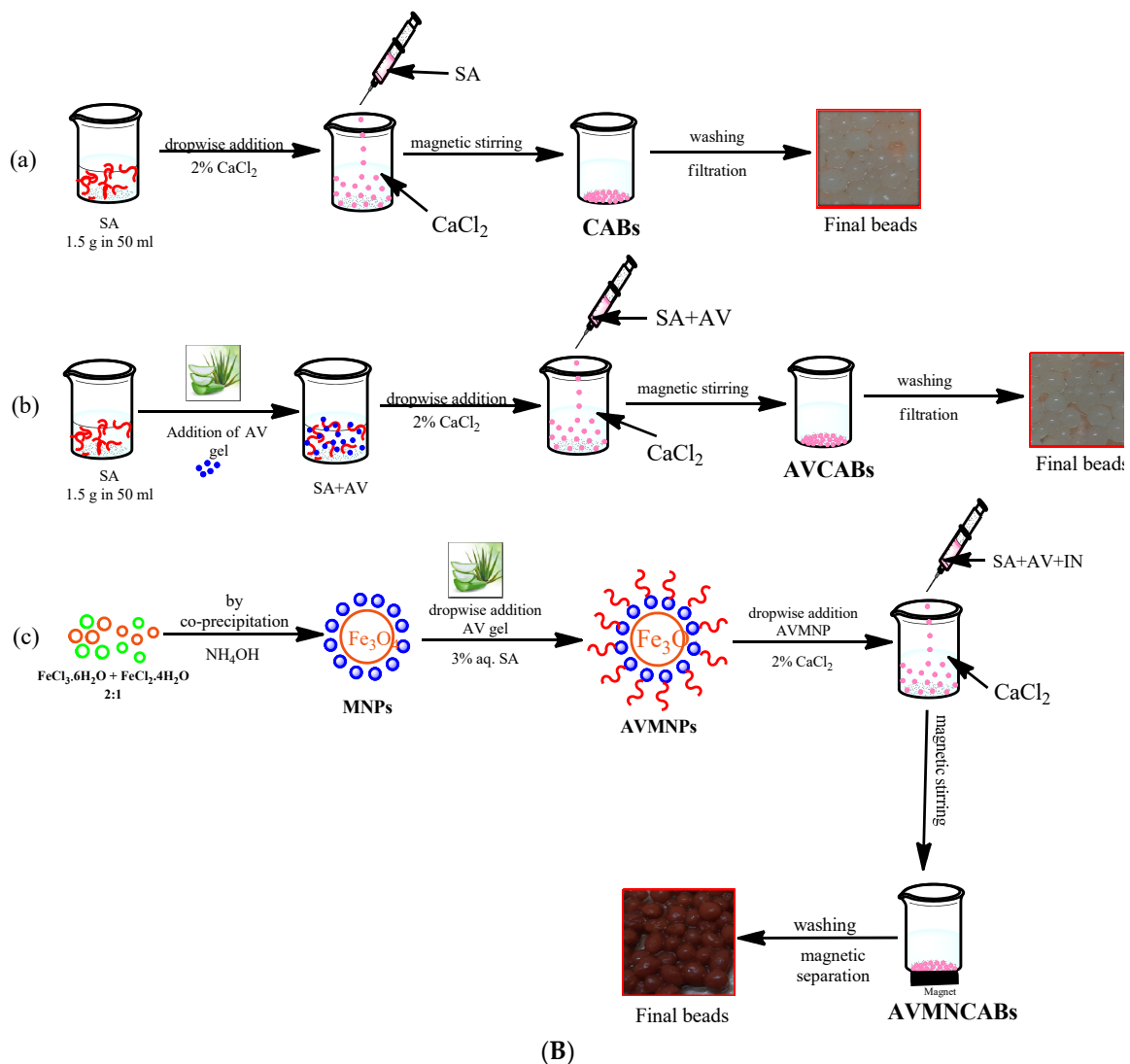


Figure 1. (A) Images of the (a) CABs, (b) AVCABs and (c) AVMNCABs gel beads (approximate size of beads: 2–3 mm); (B) Synthesis of (a) CABs, (b) AVCABs, and (c) AVMNCABs gel beads.

2.4. Spectrophotometric Determination of Cu (II)

After the adsorption, the beads were separated from the liquid by filtration, and the concentration of Cu(II) was spectrophotometrically determined using potassium thiocyanate and variamine blue. Then, 5 mL of filtrate, 0.5 mL of potassium thiocyanate (0.2 N), and 0.6 mL of a 0.05% variamine blue solution were added, which resulted in the oxidation of the leucoform of variamine blue to variamine blue (violet color), with a maximum absorbance at 550 nm. The concentration of the Cu(II) was obtained from the calibration curve [46].

2.5. Batch Adsorption Experiments

The adsorption performance of the gel beads for removing copper from aqueous solutions was investigated using a batch adsorption approach. The effects of pH (2–7), adsorbent amount (0.05–0.6 g), time of contact (5–180 min), and initial ion concentration (10–90 mg L⁻¹) on the removal efficiency were studied. The pH was adjusted by using 0.1 M HCl/0.1 M NaOH. A fixed volume of Cu(II) ion solution (10 µg mL⁻¹) was shaken with 0.2 g of CABs, AVCABs, and AVMNCABs at a pH of 4 and at 35 °C for 120 min. The adsorption isotherms were obtained by using aqueous solutions of Cu(II) with several concentrations. After the adsorption, the adsorbents were separated by filtration, and the Cu (II) amount in the filtrate was determined by UV-vis at 550 nm using potassium

thiocyanate and variamine blue. The materials were characterized using SEM-EDX, FTIR, XRD, and VSM. The percentage of removal, adsorption capacity at equilibrium (q_e), and at a given time t (q_t) were calculated using Equations (1)–(3), respectively:

$$R = \frac{C_0 - C_e}{C_0} \quad (1)$$

$$q_e (\%) = \frac{(C_0 - C_e) V}{m} \quad (2)$$

$$q_t (\%) = \frac{(C_0 - C_t) V}{m} \quad (3)$$

where C_0 , C_e , and C_t are the initial, equilibrium, and at a given t time concentrations of Cu(II) ions ($\mu\text{g mL}^{-1}$), respectively, m is the adsorbent mass (g), and V is the solution volume (L).

2.6. Desorption

The desorption was carried out using 2 mL of a 0.05 M HNO_3 solution as the desorption agent. The adsorbent was washed with double distilled water three times, and its reusability was assessed. The adsorbents exhibited good adsorption–desorption performance and could be reused up to 7 cycles (Figure 2). The desorption (%) was calculated by:

$$\text{Desorption}(\%) = \frac{\text{Desorbed quantity of metal}}{\text{Adsorbed quantity of metal}} \times 100 \quad (4)$$

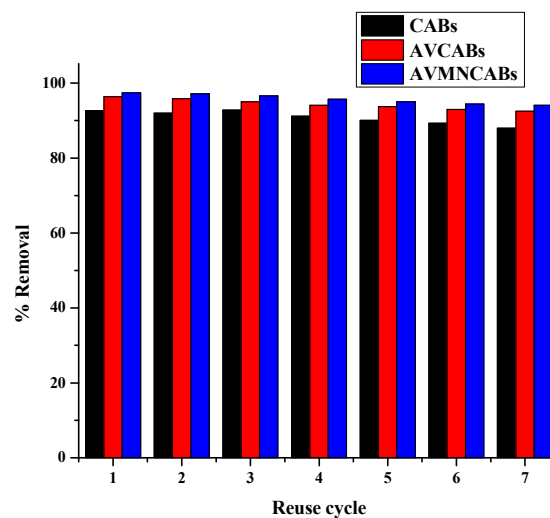


Figure 2. Reusability of CABs, AVCABs, and AVMNCABs up to 7 cycles.

92.7%, 96.4%, and 97.4% desorption were obtained for CABs, AVCABs, and AVMNCABs, respectively.

3. Results and Discussion

3.1. Adsorbent Characterization

3.1.1. X-ray Diffraction (XRD)

The XRD diffractograms of the iron oxide nanoparticles, CABs, AVCABs, and AVMNCABs show several characteristic peaks (Figure 3). The XRD pattern of CABs shows broad peaks at 2θ values of 31.80° and 36.61° , while AVCABs show comparatively sharp peaks at 2θ values of 31.87° , 34.33° , 36.25° , 43.37° , 56.69° , and 62.97° . The XRD pattern of the iron oxide nanoparticles shows broad peaks at $2\theta = 30.20^\circ$, 36.24° , 43.21° , 53.74° , 57.23° , and 62.90° , identical to the standard JCPDS data [47] for Fe_3O_4 , which can be indexed to (220), (311), (400), (422), (511), and (440) planes. The Aloe vera-alginate beads containing

iron oxide nanoparticles (AVMNCABs) show six characteristic peaks at 2θ values of 30.2° , 35.67° , 43.21° , 54.08° , 57.62° , and 62.51° , identical to that of the planes of Fe_3O_4 [48]. The narrow, sharp peaks of AVMNCABs indicate the small crystallites and ultra-fine nature of the particles and indicate the spinal structure.

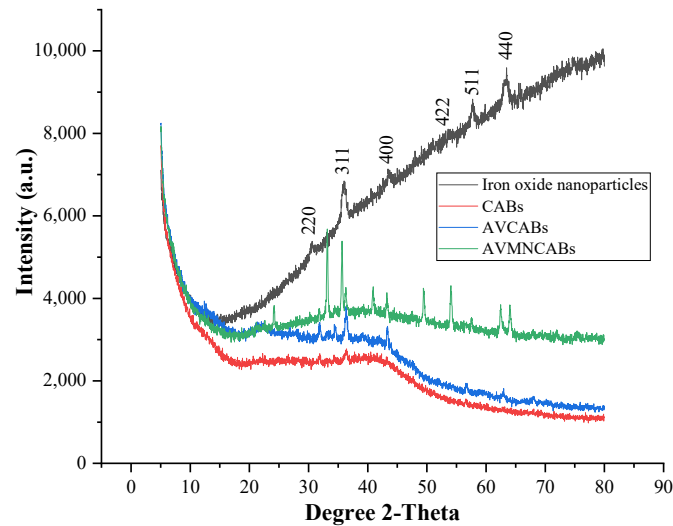


Figure 3. XRD patterns of iron oxide (Fe_3O_4) nanoparticles, CABs, AVCABs, and AVMNCABs, with the characteristic peaks of Fe_3O_4 identified.

The average crystal size of the CABs, AVCABs, and AVMNCABs were determined using Debye–Scherrer’s Equation [49]:

$$D = \frac{K \cdot \lambda}{\beta \cdot \cos\theta} \quad (5)$$

where D is the average size of crystallites in \AA , θ is the diffraction angle, β is the FWHM (full width at half maximum) of the peak, λ is the X-ray wavelength (1.54 \AA), and K is a constant ($K = 0.9 \text{ \AA}$). Table 1 shows the particle sizes of CABs, AVCABs, and AVMNCABs: 0.072 nm , 0.131 nm , and 0.022 nm , respectively.

Table 1. Average crystal size of CABs, AVCABs, and AVMNCABs calculated using Debye–Scherrer’s formula.

Samples	Most Intense Peak (2θ , Degrees)	Most Intense Peak (θ , Degrees)	FWHM of the Most Intense Peak (β , Radians)	Particle Size (D , nm)
CABs	36.61	18.30	2.00	0.072
AVCABs	36.25	18.12	1.11	0.131
AVMNCABs	33.11	16.55	6.57	0.022

3.1.2. Fourier Transform Infrared Spectroscopy (FTIR)

The FTIR spectra of the CABs, AVCABs, and AVMNCABs are displayed in Figure 4. Calcium alginate shows characteristic peaks at 3235 and 2923 cm^{-1} , attributed to O-H stretching and C-H stretching vibrations. The bands at 1588 and 1410 cm^{-1} are due to the asymmetric and symmetric vibrations of C=O of the COO^- group. The peak around 1079 cm^{-1} corresponds to C-O, C-C, and C-O-C stretching vibrations, and the sharp peak at 1022 cm^{-1} is due to C-C and C-O-C stretching [50]. The spectrum of the AVCABs shows shifts in the position and intensity of the bands due to -OH stretching (3228 cm^{-1}) and asymmetric C=O stretching vibrations (1586 cm^{-1}). In the case of AVMNCABs, the peaks

shift to 3241, 2922, and 1585 cm^{-1} . The intensity of the peaks decreases due to the chelation of OH and COO^- to the Fe^{3+} ion. An additional peak at 568 cm^{-1} is observed, which can be ascribed to Fe-O vibration.

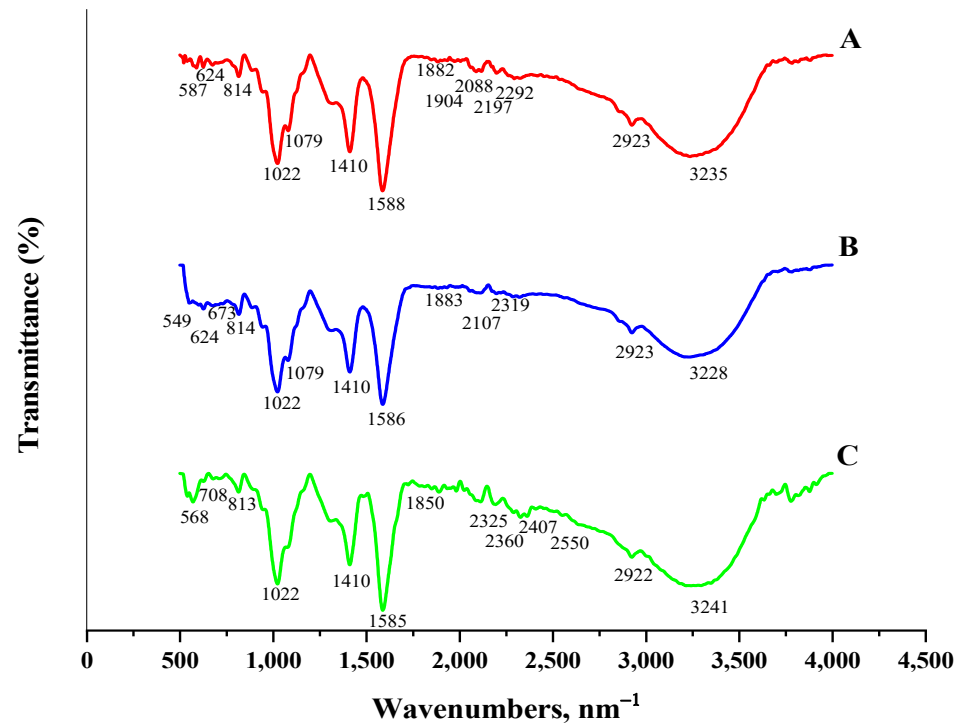


Figure 4. FTIR spectra of (A) CABs, (B) AVCABs, and (C) AVMNCABs before adsorption.

3.1.3. Vibrating Sample Magnetometer (VSM)

This technique was used to assess the magnetic properties of the materials, such as retentivity (M_R), coercivity (H_C), and saturation magnetization (M_S). The hysteresis loop describing the magnetization of CABs, AVCABs, and AVMNCABs is shown in Figure 5. The saturation magnetization measures the material magnetization extent in an external magnetic field. The coercivity is the intensity of the magnetic field needed to reduce the material magnetization to zero after the sample has been magnetized. The values of M_S are 6.77×10^{-3} , 4.89×10^{-3} , and 1.08×10^{-1} emu/g for CABs, AVCABs, and AVMNCABs, respectively, indicating the enhancement of the magnetic properties of AVMNCABs after the incorporation of iron nanoparticles, compared to CABs and AVCABs. The value of H_S is 193.15 O_e for AVMNCABs, showing the ferromagnetic nature of the AVMNCABs, whereas the other adsorbents are non-magnetic. A decrease in M_S has been reported in several adsorbents [51–53]. The obtained low value of M_S , compared to iron nanoparticles, can be explained by the presence of a non-magnetic substance in the adsorbent matrix. The appreciable magnetic properties of AVMNCABs, compared to CABs and AVCABs, enable the easy removal by the first adsorbent in less time.

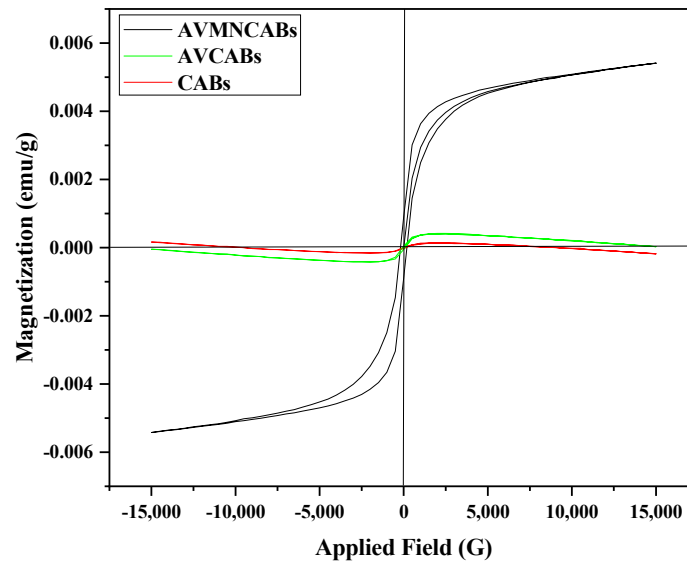


Figure 5. Vibrating sample magnetization (VSM) of CABs, AVCABs, and AVMNCABs (at room temperature).

3.1.4. Scanning Electron Microscopy (SEM)

The morphological features of the synthesized adsorbents were investigated by SEM. The images of CABs (a), AVCABs (b), and AVMNCABs (c) show the surface morphology of the various alginate beads (Figure 6). AVMNCABs are shown to have a more irregular, uneven structure, with a large surface area available for adsorption compared to the other materials. Figure 6 shows that the surface of the AVMNCABs has more pores than CABs and AVCABs, indicating the enhanced adsorption capacity of the former material (Figure 6a–c). Figure 6d shows that the surface of AVMNCABs has less porosity after adsorption, as most of the available pores found in beads are covered, causing the surface of the beads to be more saturated and smother.

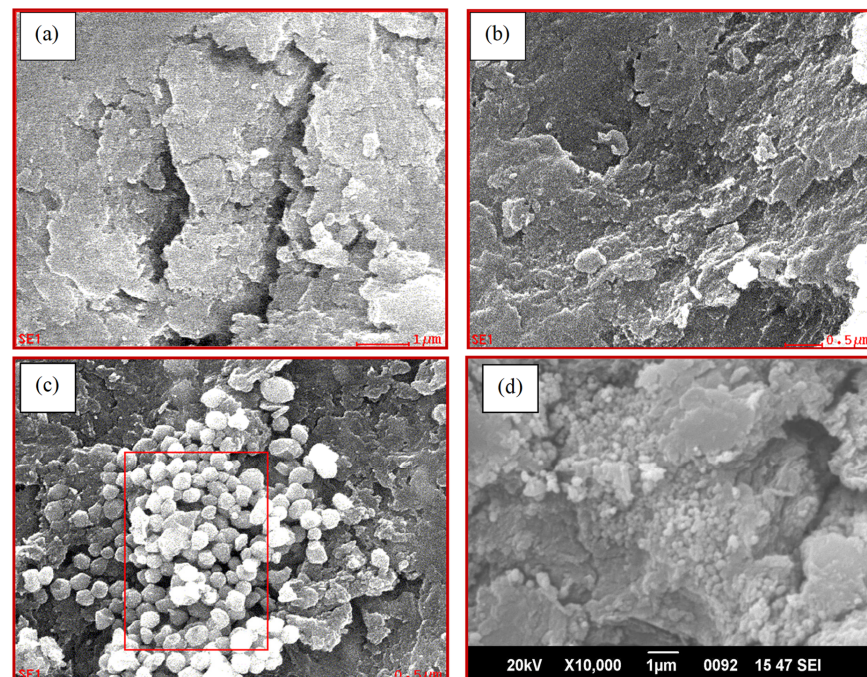


Figure 6. SEM images of (a) CABs, (b) AVCABs, and (c) AVMNCABs before adsorption and (d) AVMNCABs after adsorption.

3.1.5. Energy Dispersive X-ray (EDX) Spectroscopy

EDX was used to determine the composition of the samples. As shown in Figure 7a, CABs contain C (43.3%), O (39.21%), Na (4.44%), and Ca (12.25%). Figure 7b shows that the AVCABs have C (33.21%), O (38.38%), Na (3.35%), and Ca (24.43%), and Figure 7c indicates that AVMNCABs (after adsorption) comprise C (22.69%), O (34.30%), Na (5.51%), Ca (11.44%), and Fe (25.06%), which confirms the incorporation of iron nanoparticles onto the alginate beads. Figure 7d clearly shows the presence of Cu in the nanocomposite matrix of AVMNCABs, demonstrating the efficiency of the beads in removing Cu(II) from the water.

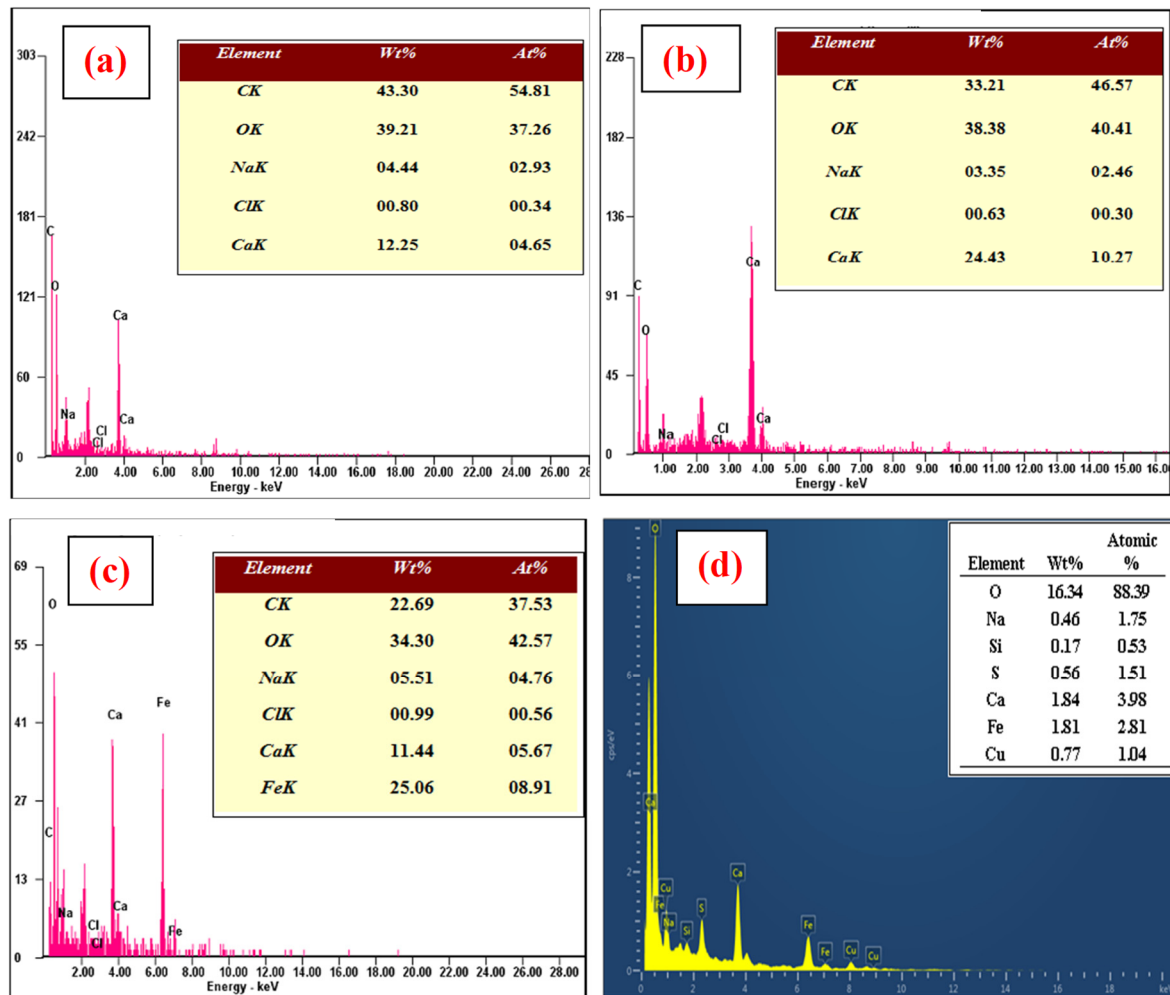


Figure 7. EDX spectra of (a) CABs, (b) AVCABs, and (c) AVMNCABs before adsorption; and (d) AVMNCABs after adsorption.

3.2. Effect of pH

The pH of the solution is a crucial factor in the removal of Cu(II). The pH was adjusted using different quantities of 0.1 M HCl or 0.1 M NaOH solutions. The influence of pH on the removal of Cu(II) was tested by changing the pH from 2 to 7 using an initial Cu(II) concentration of 10 mg L^{-1} , 0.2 g adsorbent, and a 1 h contact time. Figure 8 shows that the removal (%) increases with pH increase until pH 4. Above that value, a reduction in removal is found in all the cases.

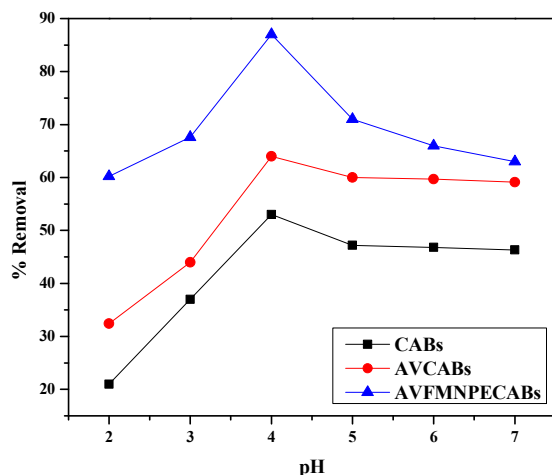


Figure 8. pH effect on Cu(II) removal for an initial concentration of $10 \mu\text{g mL}^{-1}$; 0.2 g adsorbent; 1 h.

The point of zero charge (pH_{pzc}) was 3.72 for AVMNCABs and AVCABs and 3.32 for CABs (Figure 9). For pH values below pH_{pzc} , the surface of the adsorbent has positive charges. However, for $\text{pH} > \text{pH}_{\text{pzc}}$, the surface becomes negative, which facilitates the electrostatic attraction of the copper(II) ion. The maximal adsorption of Cu(II) was observed at pH 4, which is above the pH_{pzc} value [54].

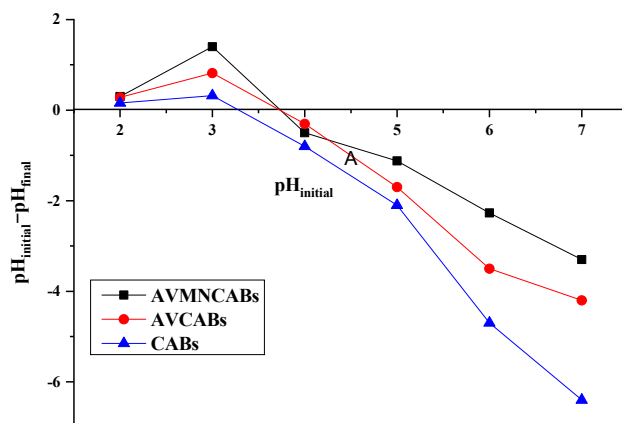


Figure 9. Point of zero charge (pH_{pzc}) of AVMNCABs, AVCABs, and CABs.

At lower pH values, the adsorbents are protonated; that is, they have a positive surface charge, which leads to strong repulsion with the also positively charged Cu(II) ions. Furthermore, for $\text{pH} > 4$, the surface active sites of the adsorbents are unprotonated, and hence, the surface has a negative charge, which increases the adsorption of Cu(II). At highly-basic pH, Cu(II) ions can precipitate in the form of insoluble hydroxides, lowering the adsorption. Moreover, the competition between Cu(II) and H^+ can also decrease adsorption. The maximum removal efficiencies for CABs, AVCABs, and AVMNCABs were 53%, 64%, and 87%, respectively, at pH 4.

3.3. Effect of Adsorbent Amount

The adsorption capacity of the materials was revealed by the variation of the adsorbent amount from 0.05 to 0.6 g (Figure 10). After a certain dose, the removal shows no significant changes. The amount of Cu(II) adsorbed by CABs, AVCABs, and AVMNCABs increased from 65.1 to 81.4%, 74.28 to 83.5%, and 79 to 89.1%, respectively, for adsorbent amounts ranging from 0.1 to 0.4 g (CABs), 0.1 to 0.5 g (AVCABs), and 0.1 to 0.2 g (AVMNCABs). The increase in the removal efficiency with the increase in the amount of adsorbent can

be correlated with a higher number of active sites on the adsorbent surface, which are accessible to the metal ions.

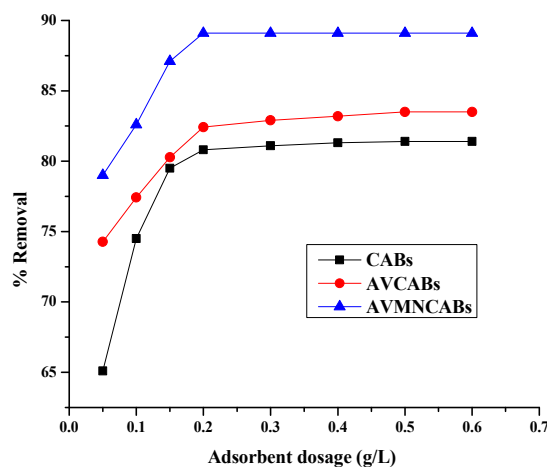


Figure 10. Variation of the removal of Cu(II) with adsorbent dose ($10 \mu\text{g mL}^{-1}$ Cu(II), 1 h, 30°C , pH 4).

3.4. Effect of Time

The influence of time on the removal of Cu(II) was determined from 5–180 min at pH 4, and the results can be found in Figure 11. The removal ranged from 25.3 to 97.6% in the time span of 5–120 min. The minimum and maximum efficiencies for CABs, AVCABs, and AVMNCABs, were 25.3–86.1%, 33.9–94.6%, and 53–97.6%, respectively, for 5 to 120 min. Initially, the adsorption process was quite fast but slowed down with time. The initial higher rate of removal could be caused by the relatively high Cu(II) concentration and a large number of vacant active surface sites on the adsorbent. The lowering of the removal rate with time can be ascribed to a decrease in the availability of the adsorbent active sites.

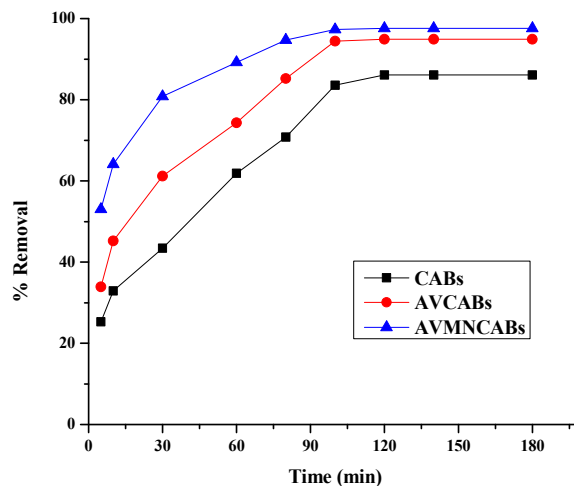


Figure 11. Effect of time on the removal of Cu(II) ($10 \mu\text{g mL}^{-1}$ Cu(II), 0.2 g adsorbent; 30°C , pH 4).

3.5. Effect of Copper Ion Concentration

Cu(II) adsorption was investigated for the previously found optimum time (120 min), pH 4, 10 to $80 \mu\text{g mL}^{-1}$ copper ion concentration. An increase in the initial value leads to an adsorption decrease. Figure 12 shows that the maximal removal of Cu(II) was 88.4% (CABs), 94.7% (AVCABs), and 98.6% (AVMNCABs). More adsorption sites are available for lower Cu(II) concentrations. As the number of Cu(II) ions increases, for higher concentrations, less active sites are available for adsorption. Hence, adsorption depends on the initial

concentration of Cu(II). As this concentration increases, more active sites are covered, and Cu(II) ions have greater competition for the surface of the adsorbent [55].

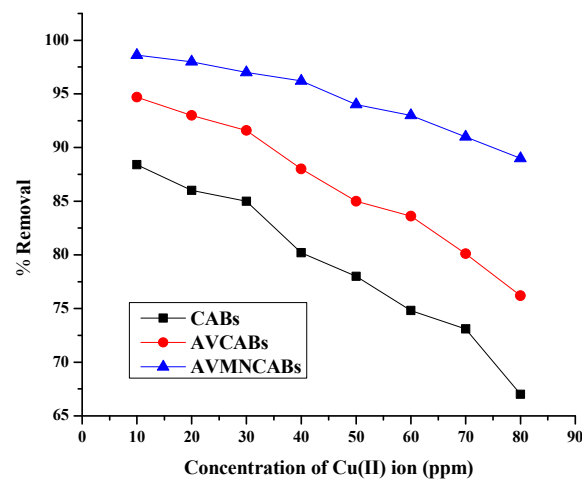


Figure 12. Effect of the initial Cu(II) concentration on the adsorption (0.2 g adsorbent, 120 min, 30 °C, pH 4).

3.6. Adsorption Isotherms

Various models of adsorption isotherms were tested to assess the adsorption capacity under optimized conditions. The acquired data were applied to the Freundlich [56], Langmuir [57], and Temkin [58] models. The adsorption parameters obtained for CABs, AVCABs, and AVMNCABs for removing Cu(II) are in Table 2.

Table 2. Parameters of the adsorption isotherm of Cu(II) on various adsorbents.

Isotherm		Value of Parameters		
Langmuir	q_{max} (mg g ⁻¹)	K_L	R^2	R_L
CABs	15.38	0.193	0.982	0.518
AVCABs	41.66	0.049	0.991	0.671
AVMNCABs	111.11	0.014	0.997	0.877
Freundlich	K_F (mg g ⁻¹) (mg L ⁻¹) ⁿ	n	R^2	
CABs	3.296	1.182	0.959	
AVCABs	2.137	1.05	0.986	
AVMNCABs	1.62	1.026	0.994	
Temkin	B_1	K_T (L mg ⁻¹)	R^2	
CABs	28.19	0.058	0.779	
AVCABs	30.99	0.03	0.837	
AVMNCABs	17.26	0.091	0.919	

The Langmuir isotherm model is characterized by the equation:

$$\frac{1}{q_e} = \frac{1}{q_m} + \frac{1}{K_m q_m} \cdot \frac{1}{C_e} \quad (6)$$

where: K_m is the Langmuir adsorption constant (L/mg), q_m is the adsorbent maximum adsorption capacity (mg/g); C_e and q_e are the equilibrium concentration of Cu(II) ion and equilibrium adsorption capacity (mg/L), respectively. The $1/q_e$ versus $1/C_e$ plot is depicted in Figure 13A.

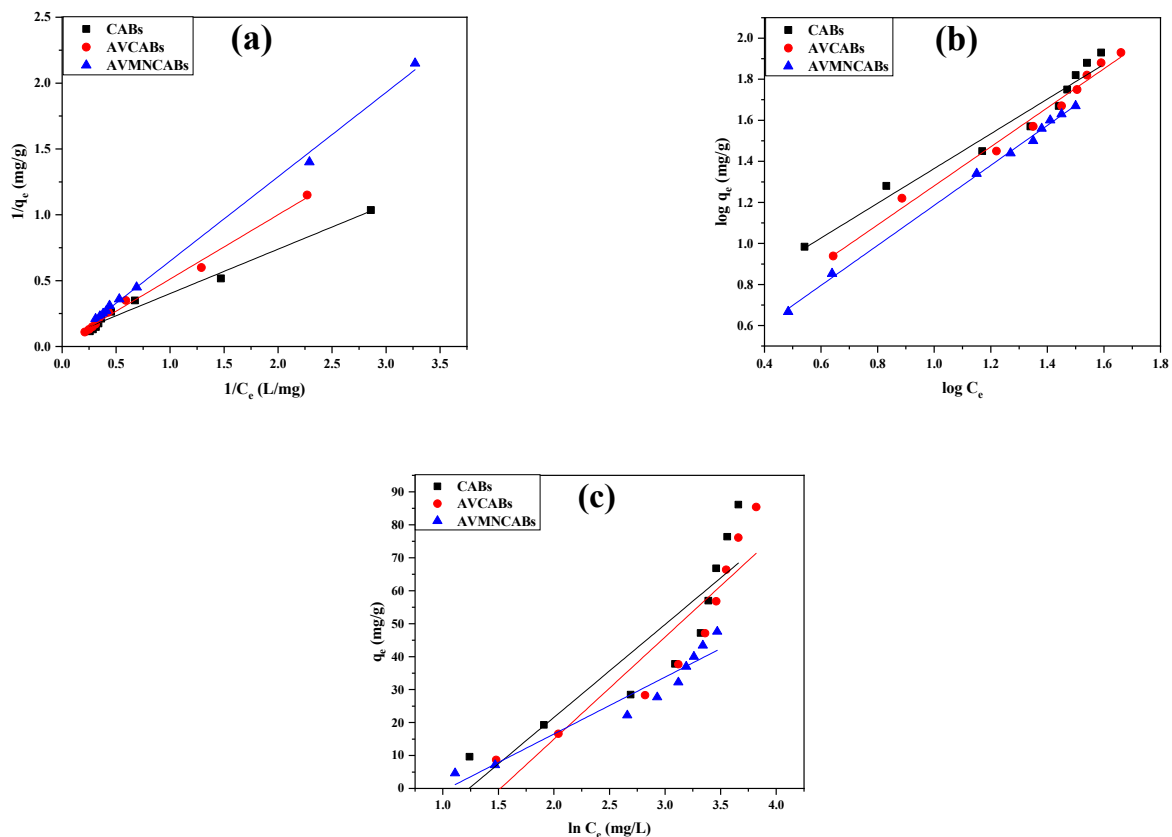


Figure 13. Adsorption isotherms: (a) Langmuir, (b) Freundlich, and (c) Temkin for CABs, AVCABs, and AVMNCABs.

The separation factor, constant, and equilibrium parameter R_L were calculated with

$$R_L = \frac{1}{1 + K_L C_0} \quad (7)$$

R_L infers if the adsorption is irreversible (for $R_L = 0$), favorable (for $0 < R_L < 1$), linear (for $R_L = 1$), or not favorable (for $R_L > 1$). In the present case, the value of R_L is much smaller than 1, confirming that Cu(II) adsorption is a favorable process [59–61].

The Freundlich model depicting multilayer adsorption is expressed as:

$$\log q_e = \log K_F + \frac{1}{n} \log C_e \quad (8)$$

where: n and K_F (L/mg) are the Freundlich constants, indicative of the intensity and adsorption capacity, respectively; q_e and C_e are the equilibrium adsorption capacity (mg/g) and equilibrium concentration of Cu(II), respectively. K_F and $1/n$ values can be obtained from the intercept and slope of the $\log q_e$ versus $\log C_e$ plot represented in Figure 13B.

The Temkin isotherm model is centered on the surface coverage. The adsorption energy decreases linearly with coverage. This isotherm is expressed by Equation (9):

$$q_e = B_1 \ln k_T + B_1 \ln c_e \quad (9)$$

where: $B_1 = RT/b$; b is the Temkin constant (J/mol); T is the temperature (K); R is the gas constant (8.314 J/mol K); B_1 is the constant related with the adsorption heat (J/mol); k_T is the constant of equilibrium binding (L/g). The determination of k_T and B_1 can be performed by the q_e versus $\ln C_e$ plot, as shown in Figure 13C.

3.7. Adsorption Kinetics

The pseudo-first-order [62], pseudo-second-order [63], Elovich kinetics [64], and intra-particle diffusion [65] models were used to investigate the adsorption kinetics. The effect of the contact time on the adsorption is presented in Figure 14 and Table 3.

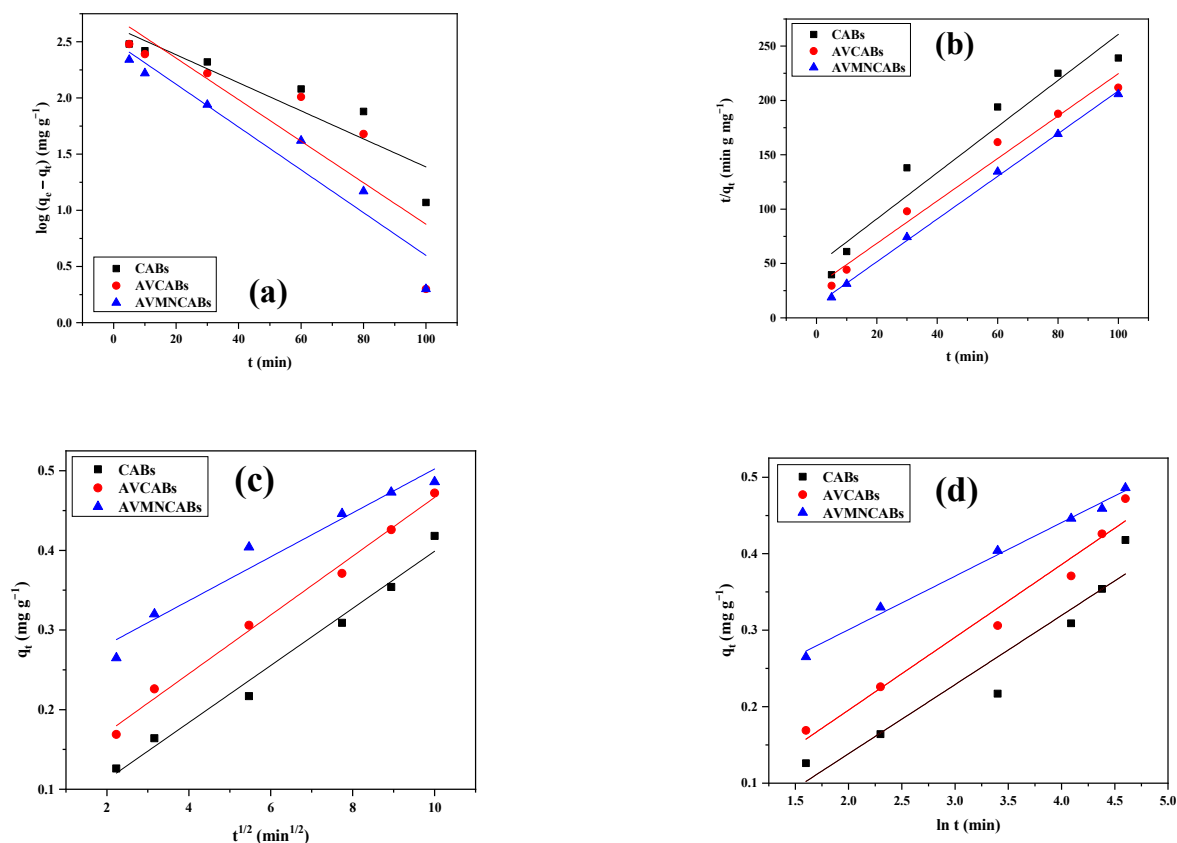


Figure 14. (a) Kinetic fittings for pseudo-first order, (b) pseudo-second order, (c) intra-particle diffusion, and (d) Elovich models.

Table 3. Kinetic parameters for Cu(II) adsorption on various adsorbents.

Models	Kinetics Parameters		
Pseudo-First-Order	k_1 (min^{-1})	q_e (mg g^{-1})	R^2
CABs	0.027	426.578	426.578
AVCABs	0.041	426.578	426.578
AVMNCABs	0.043	426.578	426.578
Pseudo-Second-Order	k_2 ($\text{g mg}^{-1} \text{min}^{-1}$)	q_e (mg g^{-1})	R^2
CABs	0.092	0.471	0.931
AVCABs	0.129	0.512	0.973
AVMNCABs	0.312	0.510	0.997
Intra-particle Diffusion	k_d ($\text{mg g}^{-1} \text{min}^{-1/2}$)	C (mg g^{-1})	R^2
CABs	0.035	0.040	0.980
AVCABs	0.036	0.097	0.991
AVMNCABs	0.027	0.226	0.949
Elovich model	α ($\text{mg g}^{-1} \text{min}^{-2}$)	β ($\text{g mg}^{-1} \text{min}^{-1}$)	R^2
CABs	-0.042	0.090	0.900
AVCABs	0.005	0.095	0.962
AVMNCABs	0.160	0.069	0.991

The pseudo-first-order, pseudo-second-order, Elovich kinetics, and intra-particle diffusion follow Equations (10)–(13).

$$\log (q_e - q_t) = \log q_e - \frac{k_1 t}{2.303} \quad (10)$$

where: q_e and q_t are the quantity of copper adsorbed (mg g^{-1}) at equilibrium and at a given time t (min), respectively; k_1 (min^{-1}) is the pseudo-first-order rate constant. The $\log (q_e - q_t)$ versus t plot is shown in Figure 14A.

$$\frac{1}{q_t} = \frac{t}{k_2 q_e^2} - \frac{1}{q_e} \quad (11)$$

where: k_2 (g/mg min^{-1}) is the pseudo-second-order rate constant; q_e and q_t are the same as above. t/q_t versus t plot is shown in Figure 14B. The highest correlation coefficient was obtained for pseudo-second-order kinetics.

The intra-particle diffusion model centered on the diffusion mechanism, suggested by Weber and Morris, is given by:

$$q_t = K_d t^{1/2} + C \quad (12)$$

where: K_d is the pores diffusion rate constant ($\text{mg/g min}^{1/2}$); C is the intercept (mg/g). The d_t versus $t^{1/2}$ plot is shown in Figure 14C.

The Elovich equation is generally used in chemisorption and satisfactorily applies to the chemisorption process; it is expressed as:

$$q_t = \alpha + \beta \ln t \quad (13)$$

where: q_t (mg/g) is the amount of copper(II) adsorbed at time t (min); α ($\text{mg g}^{-1} \text{min}^{-1}$) and β (g mg^{-1}) are constants, respectively, obtained from the intercept and the slope of q_t versus $\ln t$ linear plot, as shown in Figure 14D.

3.8. Thermodynamic Parameters

The thermodynamic parameters, namely the free energy of Gibbs (ΔG , kJ mol^{-1}), changes in enthalpy (ΔH , kJ mol^{-1}), and entropy (ΔS , $\text{J mol}^{-1} \text{K}^{-1}$) for the adsorption of Cu(II) on various beads was determined using the equilibrium data obtained at different temperatures using the Gibbs and Van't Hoff equations [66]:

$$\Delta G = -RT \ln K_d \quad (14)$$

$$\ln K_d = \frac{\Delta S}{R} - \frac{\Delta H}{RT} \quad (15)$$

where: K_d is the Langmuir equilibrium constant (L/g); T is the temperature (K); R is the gas constant (8.314 kJ/mol K). The ΔS and ΔH values can be, respectively, attained from the intercept and slope of plot $\ln K_d$ versus $1/T$ (Figure 15). The Van't Hoff equation relates the coefficient of distribution with ΔS and ΔH at a given temperature. The negative values of ΔG at 30°C , 40°C , and 50°C (Table 4), infer that Cu(II) adsorption onto various beads was thermodynamically possible and spontaneous for all of the studied temperatures. The positive enthalpy demonstrates the adsorption endothermic nature.

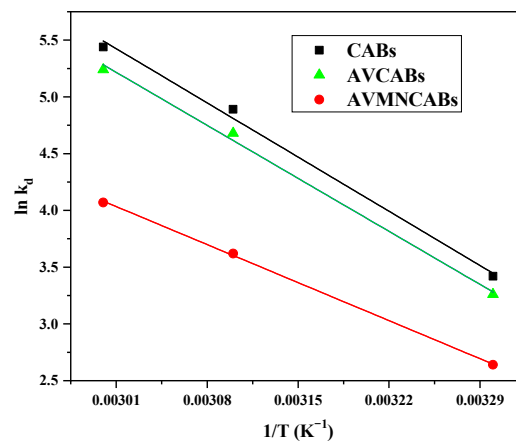


Figure 15. Van't Hoff's plot for Cu(II) adsorption.

Table 4. Thermodynamic parameters for Cu(II) adsorption on CABs, AVCABs, and AVMNCABs.

Adsorbents	ΔH (kJ/mol)	ΔS (J/mol/K)	ΔG (kJ/mol)		
			303 K	313 K	323 K
CABs	0.82	215.7	−8.6	−12.7	−14.6
AVCABs	0.8	210.2	−8.21	−12.17	−14.07
AVMNCABs	0.57	153.2	−6.6	−9.4	−10.9

3.9. Adsorption Mechanism

The FTIR spectra of the adsorbents (Figure 4) show peaks due to $-\text{OH}$, $\text{C}=\text{O}$, and COO^- stretching and $\text{Fe}-\text{O}$ vibrations which come from the active binding sites for Cu(II) adsorption. Additionally, the maximal adsorption for the AVMNCABs, AVCABs, and CABs values are observed at pH 4. The point of zero charge (pH_{pzc}) is 3.72 for AVFMNPECABs and AVCABs and 3.32 for CABs (Figure 9). The surface is negatively charged above pH_{pzc} , which facilitates the electrostatic attraction with the Cu(II) ion.

3.10. Comparison with Other Adsorption Methods

The adsorption efficiencies of the synthesized bio-sorbents were compared with the values obtained from the literature for Cu(II) removal using other materials (Table 5). It was found that our materials showed better performance, as evidenced by the adsorption capacity values. Furthermore, our functionalized adsorbents showed a greater affinity for Cu(II) compared to the non-functionalized adsorbents.

Table 5. Adsorption capacities of different adsorbents—comparison with literature.

S.No.	Adsorbents	Adsorption Capacity (mg g ⁻¹)	pH	Ref.
1.	Polyaniline/calcium alginate composite	79.0	3.0	[67]
2.	Magnetic composite gel beads (CMC/SA/graphene oxide@Fe ₃ O ₄)	55.96	5.0	[68]
3.	Nanochitosan/sodium alginate/microcrystalline cellulose beads	43.3	5.0	[69]
4.	Fluidized zeolite beads	23.3		[70]
5.	Chitosan nanoparticles-bentonite-alginate	12.21	7.0	[71]
6.	γ-Fe ₂ O ₃ nanoparticles	34.0		[72]
7.	Iminodiacetic acid-functionalized Paeonia ostii seed coats	36.6	5.0	[73]
8.	Plasma-modified activated carbon	21.4	5.0	[74]
9.	Oxidized Functionalized multiwalled carbon nanotubes	14.086		[75]
10.	Sewage sludge-based composite adsorbent diethylenetriaminepentaacetic acid	31.42	3.0	[76]
11.	(a) Calcium alginate beads (CABs)	15.38	4.0	Present study
	(b) Aloe-vera calcium alginate beads (AVCABs)	41.66	4.0	Present study
	(c) Aloe-vera functionalized magnetic nanoparticles entrapped calcium alginate beads (AVMNCABs)	111.11	4.0	Present study

4. Conclusions

The synthesized bio-sorbents CABs, AVCABs, and AVMNCABs, can be used as cost-efficient and environmentally friendly materials for removing Cu(II) from water. The adsorption studies demonstrate the applicability of the developed spectrophotometric method. The adsorption results of CABs, AVCABs, and AVMNCABs follow a Langmuir model with a maximal adsorption capacity of 15.38 mg/g, 41.66 mg/g, and 111.11 mg/g, respectively, with the sequence: AVMNCABs > AVCABs > CABs. The kinetic data indicate that the adsorption of Cu(II) on the synthesized adsorbents follows a pseudo-second-order model. Thermodynamic studies reveal the spontaneous and endothermic nature of the adsorption process. The beads demonstrate high recyclability, and the desorption efficiencies of CABs, AVCABs, and AVMNCABs were 92.7%, 96.4%, and 98.6%, respectively, on the 7th cycle.

Author Contributions: Conceptualization: S.B.M., S.A.C.C. and A.K.S.; Data curation: S.L. and S.B.M.; Formal analysis: S.L., S.B.M., S.A.C.C. and A.K.S.; Funding acquisition: A.K.S.; Investigation: S.L. and S.B.M.; Methodology: S.L., S.B.M.; Project administration: A.K.S.; Resources: A.K.S.; Supervision: S.B.M. and A.K.S.; Validation: S.B.M., S.A.C.C. and A.K.S.; Visualization: S.B.M. and S.A.C.C.; Writing—original draft: S.L. and S.B.M.; Writing—review & editing: S.A.C.C. and A.K.S. All authors have read and agreed to the published version of the manuscript.

Funding: The authors are grateful to Fundação para a Ciência e a Tecnologia (FCT), Portugal for Scientific Employment Stimulus-Institutional Call (CEEC-INST/00102/2018) and to the Associate Laboratory for Green Chemistry-LAQV financed by national funds from FCT/MCTES (UIDB/50006/2020 and UIDP/5006/2020).

Institutional Review Board Statement: Not applicable.

Informed Consent Statement: Not applicable.

Data Availability Statement: Data will be made available upon request.

Conflicts of Interest: The authors declare no conflict of interest.

References

1. Volesky, B. Detoxification of metal-bearing effluents: Biosorption for the next century. *Hydrometallurgy* **2001**, *59*, 203–216. [[CrossRef](#)]
2. Vunain, E.; Mishra, A.K.; Mamba, B.B. Dendrimers, mesoporous silicas and chitosan-based nanosorbents for the removal of heavy-metal ions: A review. *Int. J. Biol. Macromol.* **2016**, *86*, 570–586. [[CrossRef](#)] [[PubMed](#)]
3. WHO. *Copper in Drinking-Water, Background Document for Development of WHO Guidelines for Drinking-Water Quality*; WHO: Geneva, Switzerland, 2004.
4. Tong, K.S.; Kassim, M.J.; Azraa, A. Adsorption of copper ion from its aqueous solution by a novel biosorbent *Uncaria gambir*: Equilibrium, kinetics, and thermodynamic studies. *Chem. Eng. J.* **2011**, *170*, 145–153. [[CrossRef](#)]
5. Feng, N.; Guo, X.Y.; Liang, S. Adsorption study of copper (II) by chemically modified orange peel. *J. Hazard. Mater.* **2009**, *164*, 1286–1292. [[CrossRef](#)]
6. Issabayeva, G.; Aroua, M.K.; Sulaiman, N.M. Study on palm shell activated carbon adsorption capacity to remove copper ions from aqueous solutions. *Desalination* **2010**, *262*, 94–98. [[CrossRef](#)]
7. He, J.; Li, Y.; Wang, C.; Zhang, K.; Lin, D.; Kong, L.; Liu, J. Rapid adsorption of Pb, Cu and Cd from aqueous solutions by β -cyclodextrin polymers. *Appl. Surf. Sci.* **2017**, *426*, 29–39. [[CrossRef](#)]
8. Wang, S.; Peng, Y. Natural zeolites as effective adsorbents in water and wastewater treatment. *Chem. Eng. J.* **2010**, *156*, 11–24. [[CrossRef](#)]
9. Hebeish, A.; Ramadan, M.; Abdel-Halim, E.; Abo-Okeil, A. An effective adsorbent based on sawdust for removal of direct dye from aqueous solutions. *Clean Technol. Environ. Policy* **2011**, *13*, 713–718. [[CrossRef](#)]
10. Chouchene, A.; Jeguirim, M.; Trouve, G. Biosorption performance, combustion behavior, and leaching characteristics of olive solid waste during the removal of copper and nickel from aqueous solutions. *Clean Technol. Environ. Policy* **2014**, *16*, 979–986. [[CrossRef](#)]
11. Wang, F.; Pan, Y.; Cai, P.; Guo, T.; Xiao, H. Single and binary adsorption of heavy metal ions from aqueous solutions using sugarcane cellulose-based adsorbent. *Bioresour. Technol.* **2017**, *241*, 482–490. [[CrossRef](#)]
12. Li, Y.; Xiao, H.; Pan, Y.; Wang, L. Novel Composite Adsorbent Consisting of Dissolved Cellulose Fiber/Microfibrillated Cellulose for Dye Removal from Aqueous Solution. *ACS Sustain. Chem. Eng.* **2018**, *6*, 6994–7002. [[CrossRef](#)]
13. Wang, X.; Yu, S.; Chen, Z.; Zhao, Y.; Jin, J.; Wang, X. Complexation of radionuclide $^{152+154}\text{Eu(III)}$ with alumina-bound fulvic acid studied by batch and time-resolved laser fluorescence spectroscopy. *Sci. China Chem.* **2017**, *60*, 107–114. [[CrossRef](#)]
14. Xie, Y.; Chen, C.; Ren, X.; Wang, X.; Wang, H.; Wang, X. Emerging natural and tailored materials for uranium-contaminated water treatment and environmental remediation. *Mater. Sci.* **2019**, *103*, 180–234. [[CrossRef](#)]
15. Wu, Y.; Pang, H.; Liu, Y.; Wang, X.; Yu, S.; Fu, D. Environmental remediation of heavy metal ions by novel-nanomaterials: A review. *Environ. Pollut.* **2019**, *246*, 608–620. [[CrossRef](#)]
16. Gupta, V.K.; Imran, A. Removal of lead and chromium from wastewater using bagasse fly ash—A sugar industry waste. *J. Colloid Interface Sci.* **2004**, *27*, 21–28. [[CrossRef](#)]
17. Monser, L.; Adhoum, N. Modified activated carbon for the removal of copper, zinc, chromium and cyanide from wastewater. *Sep. Purif. Technol.* **2002**, *26*, 137–146. [[CrossRef](#)]
18. Chen, J.P.; Wu, S.N.; Chong, K.H. Surface modification of a granular activated carbon by citric acid for enhancement of copper adsorption. *Carbon* **2003**, *41*, 1979–1986. [[CrossRef](#)]
19. Jjagwe, J.; Olupot, P.W.; Menya, E.; Kalibbala, H.M. Synthesis and Application of Granular Activated Carbon from Biomass Waste Materials for Water Treatment: A Review. *J. Bioresour. Bioprod.* **2021**, *6*, 292–322. [[CrossRef](#)]
20. Saad, E.M.; Elshaarawy, R.F.; Mahmoud, S.A.; El-Moselhy, K.M. New *Ulva lactuca* algae based chitosan Bio-composites for bioremediation of Cd(II) ions. *J. Bioresour. Bioprod.* **2021**, *6*, 223–242. [[CrossRef](#)]
21. Haroun, A.; El-Halawany, N. Preparation and evaluation of novel interpenetrating polymer network-based on newspaper pulp for removal of copper ions. *Polym. Plast. Technol.* **2011**, *50*, 232–238. [[CrossRef](#)]
22. Haroun, A.; Mashaly, H.; El-Sayed, N. Novel nanocomposites based on gelatin/HPET/chitosan with high performance acid red 150 dye adsorption. *Clean Technol. Environ. Policy* **2013**, *15*, 367–374. [[CrossRef](#)]
23. Kardam, A.; Raj, K.; Srivastava, S.; Srivastava, M. Nanocellulose fibers for biosorption of cadmium, nickel, and lead ions from aqueous solution. *Policy Clean Technol. Environ.* **2014**, *16*, 385–393. [[CrossRef](#)]
24. Huang, Q.; Liu, M.; Mao, L.; Xu, D.; Zeng, G.; Huang, H. Surface functionalized SiO₂ nanoparticles with cationic polymers via the combination of mussel inspired chemistry and surface initiated atom transfer radical polymerization: Characterization and enhanced removal of organic dye. *J. Colloid Interface Sci.* **2017**, *499*, 170–179. [[CrossRef](#)] [[PubMed](#)]
25. Huang, Q.; Liu, M.; Chen, J.; Wan, Q.; Tian, J.; Huang, L. Facile preparation of MoS₂ based polymer composites via mussel inspired chemistry and their high efficiency for removal of organic dyes. *Appl. Surf. Sci.* **2017**, *419*, 35–44. [[CrossRef](#)]
26. Zhang, X.; Huang, Q.; Liu, M.; Tian, J.; Zeng, G.; Li, Z. Preparation of amine functionalized carbon nanotubes via a bioinspired strategy and their application in Cu²⁺ removal. *Appl. Surf. Sci.* **2015**, *343*, 19–27. [[CrossRef](#)]
27. Kahraman, S.; Dogan, N.; Erdemoglu, S. Use of various agricultural wastes for the removal of heavy metal ions. *Int. J. Environ. Pollut.* **2008**, *34*, 275–284. [[CrossRef](#)]
28. Malkhede, S.S.; Rao, Y.R.M. Sorption of Cu (II) Ions by Adsorption using Orange Peel. *Int. Conf. Res. Front. Sci.* **2021**, *1913*, 012090.

29. Onundi, Y.B.; Mamun, A.A.; Al Khatib, M.F.; Ahmed, Y.M. Adsorption of copper, nickel and lead ions from synthetic semiconductor industrial wastewater by palm shell activated carbon. *Int. J. Environ. Sci. Technol.* **2010**, *7*, 751. [[CrossRef](#)]
30. Acar, F.N.; Eren, Z. Removal of Cu(II) ions by activated poplar sawdust (Samsun clone) from aqueous solutions. *J. Hazard. Mater.* **2006**, *137*, 909–914. [[CrossRef](#)]
31. Demirbas, E.; Dizge, N.; Sulak, M.T.; Kobya, M. Adsorption kinetics and equilibrium of copper from aqueous solutions using hazelnut shell activated carbon. *Chem. Eng. J.* **2009**, *148*, 480–487. [[CrossRef](#)]
32. Zhang, J.H.; Fu, H.; Lv, X.S.; Tang, J.; Xu, X.H. Removal of Cu(II) from aqueous solution using the rice husk carbons prepared by the physical activation process. *Biomass Bioenergy* **2011**, *35*, 464–472. [[CrossRef](#)]
33. Kim, J.W.; Sohn, M.H.; Kim, D.S.; Sohn, S.M.; Kwon, Y.S. Production of granular activated carbon from waste walnut shell and its adsorption characteristics for Cu(2+) ion. *J. Hazard. Mater.* **2001**, *85*, 301–315. [[CrossRef](#)]
34. Zhou, L.; Wang, Y.; Liu, Z.; Huang, Q. Characteristics of equilibrium, kinetics studies for adsorption of Hg(II), Cu(II), and Ni(II) ions by thiourea-modified magnetic chitosan microspheres. *J. Hazard. Mater.* **2009**, *161*, 995–1002. [[CrossRef](#)] [[PubMed](#)]
35. Tran, H.V.; Tran, L.D.; Nguyen, T.N. Preparation of chitosan/magnetite composite beads and their application for removal of Pb(II) and Ni(II) from aqueous solution. *Mater. Sci. Eng. C* **2010**, *30*, 304–310. [[CrossRef](#)]
36. Zhou, L.; Liu, Z.; Liu, J.; Huang, Q. Adsorption of Hg(II) from aqueous solution by ethylenediamine-modified magnetic crosslinking chitosan microspheres. *Desalination* **2010**, *258*, 41–47. [[CrossRef](#)]
37. Lakouraj, M.M.; Hasanadeh, F.; Zare, E.N. Nanogel and super-paramagnetic nanocomposite of thiacalix[4]arene functionalized chitosan: Synthesis, characterization and heavy metal sorption. *Iran. Polym. J.* **2014**, *23*, 933–945. [[CrossRef](#)]
38. Bezbaruah, A.N.; Krajangpan, S.; Chisholm, B.J.; Khan, E.; Bermudez, J.J.E. Entrapment of iron nanoparticles in calcium alginate beads for groundwater remediation applications. *J. Hazard. Mater.* **2009**, *166*, 1339–1343. [[CrossRef](#)]
39. Lakouraj, M.M.; Mojerlou, F.; Zare, E.N. Nanogel and superparamagnetic nanocomposite based on sodium alginate for sorption of heavy metal ions. *Carbohydr. Polym.* **2014**, *106*, 34–41. [[CrossRef](#)]
40. Badruddoza, A.Z.; Rahman, M.T.; Ghosh, S.; Hossain, M.Z.; Shi, J.Z.; Hidajat, K.; Uddin, M.S. β -Cyclodextrin conjugated magnetic, fluorescent silica core-shell nanoparticles for biomedical applications. *Carbohydr. Polym.* **2013**, *95*, 449–457. [[CrossRef](#)]
41. Zhang, X.B.; Wang, Y.; Yang, S.T. Simultaneous removal of Co(II) and 1-Naphthol by core-shell structured Fe₃O₄@cyclodextrin magnetic nanoparticles. *Carbohydr. Polym.* **2014**, *114*, 521–529. [[CrossRef](#)]
42. Shi, T.; Xie, Z.; Mo, X.; Feng, Y.; Peng, T.; Song, D. Highly efficient adsorption of heavy metals and cationic dyes by smart functionalized sodium alginate hydrogels. *Gels* **2022**, *8*, 343. [[CrossRef](#)] [[PubMed](#)]
43. Veglio, F.; Esposito, A.; Reverberi, A.P. Copper adsorption on calcium alginate beads: Equilibrium pH-related models. *Hydrometallurgy* **2002**, *65*, 43–57. [[CrossRef](#)]
44. Singh, K.; Sharma, S.K.; Jain, A.K.; Mandal, M.M.; Pandey, P.K. Removal of copper ion from synthetic wastewater using Aloe vera as an adsorbent. *Eur. J. Adv. Eng. Technol.* **2017**, *4*, 249–254.
45. Kapashi, E.; Kapnisti, M.; Dafnomili, A.; Noli, F. Aloe Vera as an effective biosorbent for the removal of thorium and barium from aqueous solutions. *J. Radioanal. Nucl. Chem.* **2019**, *321*, 217–226. [[CrossRef](#)]
46. Lilhare, S.; Mathew, S.B.; Singh, A.K. A novel chromogenic scheme for the determination of Cu(II) in water samples. *Anal. Chem. Lett.* **2021**, *11*, 872–885. [[CrossRef](#)]
47. JCPDS Data Card. *International Center of Diffraction Data*; National Bureau of Standards: Washington, DC, USA, 1988.
48. Verma, R.; Asthana, A.; Singh, A.K.; Susan, M.A.B.H. Glycine functionalized magnetic nanoparticle entrapped calcium alginate beads: A promising adsorbent for removal of Cu(II) ions. *J. Environ. Chem. Eng.* **2016**, *4*, 1985–1995.
49. Singh, M.; Dosanjh, H.S.; Singh, H. Surface modified spinel cobalt ferrite nanoparticles for cationic dye removal: Kinetics and thermodynamics studies. *J. Water Process Eng.* **2016**, *11*, 152–161. [[CrossRef](#)]
50. Nastaj, J.; Przewłocka, A.; Rajkowska-Myśliwiec, M. Biosorption of Ni(II), Pb(II) and Zn(II) on calcium alginate beads: Equilibrium, kinetic and mechanism studies. *Pol. J. Chem. Technol.* **2016**, *18*, 81–87. [[CrossRef](#)]
51. Reddy, D.H.; Lee, S.M. Application of magnetic chitosan composites for the removal of toxic metal and dyes from aqueous solutions. *Adv. Colloid Interface Sci.* **2013**, *201*, 68–93. [[CrossRef](#)]
52. Mirjavadi, E.S.; Tehrani, R.M.A.; Khadir, A. Effective adsorption of zinc on magnetic nanocomposite of Fe₃O₄/zeolite/cellulose nanofibers: Kinetic, equilibrium, and thermodynamic study. *Environ. Sci. Pollut. Res. Int.* **2019**, *26*, 33478–33493. [[CrossRef](#)]
53. Verma, R.; Asthana, A.; Singh, A.K.; Prasad, S.; Susan, M.A.B.H. Novel glycine-functionalized magnetic nanoparticles entrapped calcium alginate beads for effective removal of lead. *Microchem. J.* **2017**, *130*, 168–178. [[CrossRef](#)]
54. Ai, L.; Huang, H.Y.; Chen, Z.L.; Wei, X.; Jiang, J. Activated carbon/CoFe₂O₄ composites: Facile synthesis, magnetic performance and their potential application for the removal of malachite green from water. *Chem. Eng. J.* **2010**, *156*, 243–249. [[CrossRef](#)]
55. Fotsing, P.N.; Woumfo, E.D.; Măicăneanu, S.A.; Vieillard, J.; Theka, C.; Nguéagni, P.T.; Siéwé, J.M. Removal of Cu(II) from aqueous solution using a composite made from cocoa cortex and sodium alginate. *Environ. Sci. Pollut. Res.* **2020**, *27*, 8451–8466. [[CrossRef](#)] [[PubMed](#)]
56. Freundlich, H.M.F. Over the Adsorption in Solution. *J. Phys. Chem.* **1906**, *57*, 385–471.
57. Langmuir, I. The constitution and fundamental properties of Solid and Liquids. Part I. Solids. *J. Am. Chem. Soc.* **1916**, *38*, 2221–2295. [[CrossRef](#)]
58. Temkin, M.; Pyzhev, V. Kinetics of Ammonia Synthesis on Promoted Iron Catalysts. *Acta Physicochim* **1940**, *12*, 327–356.

59. Naghizadeh, A.; Ghasemi, F.; Derakhshani, E.; Shahabi, H. Thermodynamic, kinetic and isotherm studies of sulfate removal from aqueous solutions by graphene and graphite nanoparticles. *Desalin. Water Treat.* **2017**, *80*, 247–254. [[CrossRef](#)]
60. Naghizadeh, A.; Gholami, K. Bentonite and montmorillonite nanoparticles effectiveness in removal of fluoride from water solutions. *J. Water Health* **2017**, *15*, 555–565. [[CrossRef](#)]
61. Kamranifar, M.; Naghizadeh, A. Montmorillonite Nanoparticles in Removal of Textile Dyes from Aqueous Solutions: Study of Kinetics and Thermodynamics. *Iran. J. Chem. Chem. Eng.* **2017**, *36*, 127–137.
62. Lagergren, S. About the theory of so-called adsorption of soluble substances. *Kungl. Sven. Vetensk. Handlingar.* **1898**, *24*, 1–39.
63. Ho, Y.S.; McKay, G. The Sorption of Lead(II) Ions on Peat. *Water Res.* **1999**, *33*, 578–584. [[CrossRef](#)]
64. Chien, S.H.; Layton, W.R. Application of Elovich Equation to the Kinetics of Phosphate Release and Sorption in Soils. *Soil Sci. Soc. Am. J.* **1980**, *44*, 265–268. [[CrossRef](#)]
65. Wu, F.C.; Tseng, R.L.; Juang, R.S. Initial behavior of intraparticle diffusion model used in the description of adsorption kinetics. *Chem. Eng. J.* **2009**, *153*, 1–8. [[CrossRef](#)]
66. Mohan, D.; Singh, K.P. Single- and multi-component adsorption of cadmium and zinc using activated carbon derived from bagasse—An agricultural waste. *Water Res.* **2002**, *36*, 2304–2315. [[CrossRef](#)]
67. Jiang, N.N.; Xu, Y.T.; Dai, Y.Q.; Luo, W.A.; Dai, L.Z. Polyaniline nanofibers assembled on alginate microsphere for Cu²⁺ and Pb²⁺ uptake. *J. Hazard. Mater.* **2012**, *215*, 17–24. [[CrossRef](#)]
68. Wu, Z.; Deng, W.; Zhou, W.; Luo, J. Novel magnetic polysaccharide/graphene oxide @FeO gel beads for adsorbing heavy metal ions. *Carbohydr. Polym.* **2019**, *216*, 119–128. [[CrossRef](#)]
69. Vijayalakshmi, K.; Gomathi, T.; Latha, S.; Hajeeth, T.; Sudha, P.N. Removal of copper (II) from aqueous solution using nanochitosan/sodium alginate/microcrystalline cellulose beads. *Int. J. Biol. Macromol.* **2016**, *82*, 440–452. [[CrossRef](#)]
70. Jovanovic, M.; Grbavcic, Z.; Rajic, N.; Obradovic, B. Removal of Cu(II) from aqueous solutions by using fluidized zeolite A beads: Hydrodynamic and sorption studies. *Chem. Eng. Sci.* **2014**, *117*, 85–92. [[CrossRef](#)]
71. Rahmani, O.; Bouzid, B.; Guibadj, A. Extraction and characterization of chitin and chitosan: Applications of chitosan nanoparticles in the adsorption of copper in an aqueous environment. *e-Polymers* **2017**, *17*, 383–397. [[CrossRef](#)]
72. Rajput, S.; Singh, L.P.; Pittman, C.U.; Mohan, D. Lead (Pb²⁺) and copper (Cu²⁺) remediation from water using superparamagnetic maghemite (γ-Fe₂O₃) nanoparticles synthesized by Flame Spray Pyrolysis (FSP). *J. Colloid Interface Sci.* **2017**, *492*, 176–190. [[CrossRef](#)]
73. Liu, Q.; Han, R.; Qu, L.; Ren, B. Enhanced adsorption of copper ions by phosphoric acid-modified Paeonia ostii seed coats. *Environ. Sci. Pollut. Res.* **2019**, *41*, 1126–1135. [[CrossRef](#)] [[PubMed](#)]
74. Wu, L.; Wan, W.; Shang, Z.; Gao, X.; Kobayashi, N.; Luo, G.; Li, Z. Surface modification of phosphoric acid activated carbon by using non-thermal plasma for enhancement of Cu(II) adsorption from aqueous solutions. *Sep. Purif. Technol.* **2018**, *197*, 156–169. [[CrossRef](#)]
75. Šolić, M.; Maletić, S.; Isakovski, M.K.; Nikić, J.; Watson, M.; Kónya, Z.; Tričković, J. Comparing the Adsorption Performance of Multiwalled Carbon Nanotubes Oxidized by Varying Degrees for Removal of Low Levels of Copper, Nickel and Chromium(VI) from Aqueous Solutions. *Water* **2020**, *12*, 723. [[CrossRef](#)]
76. Saleem, A.; Hong, W.J.; Sun, T.; Sharaf, F.; Haris, M.; Lei, S. Enhanced and selective adsorption of Copper ions from acidic conditions by diethylenetriaminepentaacetic acid-chitosan sewage sludge composite. *J. Environ. Chem. Eng.* **2020**, *8*, 104430. [[CrossRef](#)]